Bulachite, $[Al_6(AsO_4)_3(OH)_9(H_2O)_4]\cdot 2H_2O$ from Cap Garonne, France: Crystal structure and formation from a higher hydrate .

I.E. Grey[1]*, E. Yoruk[2], S. Kodjikian[2], H. Klein[2], C. Bougerol[2], H. E.A. Brand[3], P. Bordet[2], W.G Mumme[1], G. Favreau[4] and S.J. Mills[5].

[1]CSIRO Mineral Resources, Private Bag 10, Clayton South, Victoria 3169, Australia.
[2]Université Grenoble Alpes and CNRS, Institut Néel, 38000, Grenoble, France
[3]Australian Synchrotron, 800 Blackburn Road, Clayton, Victoria 3168, Australia
[4]421 avenue Jean Monnet, 13090 Aix-en-Provence, France.
[5]Geosciences, Museums Victoria, GPO Box 666, Melbourne, Victoria 3001, Australia

Abstract

Bulachite specimens from Cap Garonne, France, comprise two intimately mixed hydrated aluminium arsenate minerals with the same Al:As ratio of 2:1 and with different water contents. The crystal structures of both minerals have been solved using data from low-dose electron diffraction tomography combined with synchrotron powder X-ray diffraction. One of the minerals has the same PXRD pattern as for published bulachite. It has orthorhombic symmetry, space group *Pnma* with unit cell parameters a = 15.3994(3), b = 17.6598(3), c = 7.8083(1) Å and Z = 4, with the formula $[Al_6(AsO_4)_3(OH)_9(H_2O)_4]\cdot 2H_2O$. The second mineral is a higher hydrate with composition $[Al_6(AsO_4)_3(OH)_9(H_2O)_4]\cdot 8H_2O$. It has the same *Pnma* space group and unit cell parameters a = 19.849(2), b = 17.6903(4) and c = 7.7788(3) Å. i.e. almost the same b and c parameters but a much larger a parameter. The structures are based on polyhedral layers, parallel to (100), of composition $[Al_6(AsO_4)_3(OH)_9(H_2O)_4]$ and with H-bonded H_2O between the layers. The layers contain [001] spiral chains of edge-shared octahedra, decorated with corner connected AsO_4 tetrahedra that are the same as in the mineral liskeardite. The spiral chains are joined together by octahedral edge-sharing to form layers parallel to (100). Synchrotron PXRD patterns collected at different temperatures during heating of the specimen show that the higher-hydrate mineral starts transforming to bulachite when heated to 50°C, and the transformation is complete between 75 and 100°C.

*Email: ian.grey@csiro.au

Introduction

Bulachite, from Neubulach, northern Black Forest, Germany was first described by Walenta (1983). It occurs as aggregates of fine white needles encrusting quartz and associated with arsenocrandallite, malachite, bariopharmacosiderite and goethite. Walenta provided results from chemical and thermogravimetric analyses and powder X-ray diffraction (PXRD), that established the ideal composition as $Al_2(AsO_4)(OH)_3(H_2O)_3$ and the symmetry as orthorhombic with unit cell parameters a = 15.53, b = 17.78 and c = 7.03 Å. A second occurrence of bulachite from Sardinia, Italy, was reported by Frau and Da Pelo (2001). The Sardinian specimens were collected at a mine dump from old workings in an arsenopyrite lens in the Sa Bidda Beccia area located about 20 km southwest of Cagliari in southern Sardinia. Here the mineral occurs as whitish, satiny, polycrystalline aggregates, usually on dark-brown layers of mansfieldite and goethite encrusting quartzite clasts. Scanning electron microscope (SEM) images show that the bulachite occurs as sub-parallel groups of very thin fibres, to 150 μm long and less than 0.25 μm in diameter. Frau and Da Pelo (2001) indexed the PXRD pattern using the unit cell reported by Walenta (1983). They suggested that bulachite could have formed by direct precipitation from iron-depleted drainage waters, or alternatively, from the hydration of mansfieldite in the presence of aqueous aluminium. The most recent occurrence of bulachite is from the South mine of the Cap Garonne (CG) old copper mine near the town of Le Pradet in the Var, southeastern France, where it occurs in close association with bariopharmacoalumite-*Q*2*a*2*b*2*c* (Grey *et al*., 2014).

As part of an ongoing characterisation of hydrated Al arsenate minerals (Grey *et al*., 2013, 2014, 2015, 2016*a*,*b*) we studied specimens of bulachite from Cap Garonne where the mineral forms patchy crusts of ultrathin lath-like crystals on yellow crystals of pharmacoalumite (Figure 1). The ruler-shaped laths are typically up to 50 μm long by 0.4 μm wide and only 0.1 μm thick. A surprising result was that PXRD patterns of the specimens, while having a number

of sharp peaks in common with the pattern reported by Walenta (1987), did not have the strongest bulachite peak at 7.78 Å but had a number of broad peaks not present in the Walenta pattern, including a strong peak at $d \sim 10$ Å. Electron diffraction (ED) patterns on flat laths gave in-plane orthogonal dimensions of 17.7 Å x 7.8 Å with the 7.8 Å axis aligned along the long dimension. The ED patterns assisted in the indexing of the PXRD pattern, giving an orthorhombic unit cell with $a \approx 19.9$, $b \approx 17.7$ and $c \approx 7.8$ Å and possible space groups *Pnma* or $Pn2_1a$.

An exception to the PXRD findings was obtained in a synchrotron PXRD data collection made on small clumps of crystal aggregates packed in a capillary. Rotation of the capillary during the experiment accidentally caused the bulk of the sample to move along the capillary out of the beam, so the diffraction pattern was obtained only for crystals from the outer surface of the small clumps that had adhered to the inner wall of the capillary. The resulting PXRD pattern was the same as that reported by Walenta (1983) for bulachite. This experiment suggested that the crusts of crystals have bulachite only at the surface and a different phase in the bulk, with the possibility that bulachite has formed from the bulk specimen by reaction at the surface. To test this hypothesis we obtained synchrotron PXRD data collections on a specimen that was heated at different temperatures. Above 50°C the diffraction pattern corresponding to the above-reported cell started changing and between 75°C and 100°C it had transformed completely to the pattern reported by Walenta (1983) for bulachite.

ED patterns obtained for the sample heated to 100°C gave an orthorhombic cell with $a \approx 15.4$, $b \approx 17.7$ and $c \approx 7.8$ Å and possible space groups *Pnma* or $Pn2_1a$. i.e. the unit cell is the same as for the phase before heating, except for a large decrease in *a*. The *a* axis is normal to the ruler-shaped laths. The large decrease in *a* under very mild heating conditions is consistent with a layer structure having interlayer water molecules which are evolved on heating above ~50° C, resulting in a contraction of the interlayer separation.

We report here the application of synchrotron PXRD and precession ED methods to determine the structures of both bulachite and the higher-hydrate precursor mineral that transforms to bulachite on dehydration.

Experimental

The specimens for study were collected by GF in Salle B, South mine, Cap Garonne, Var, France (43°4'53"N, 6°1'55"E; Favreau and Galea-Clolus, 2014). The specimens were checked for chemical purity by energy-dispersive X-ray analysis in a scanning electron microscope (Figure 2). The only metals detected were Al and As, in an atomic ration of 2:1, consistent with the formula obtained by Walenta (1983). The sample is preserved in the mineralogical collections of Geosciences, Museums Victoria, registration number M55455. A sample of the type specimen of bulachite that was studied by Walenta (1983) was supplied by Thomas Theye. It was in the form of sub-millimetre tufts of densely packed fibrous crystals, see Figure 4 in Walenta (1983).

PXRD

Laboratory PXRD scans showed that even light grinding of the specimens resulted in loss of long-range ordering (severe peak broadening) so for the synchrotron experiments, small unground clumps of subparallel fibres, such as shown in Figure 2 were packed into a 0.5 mm diameter quartz capillary. In one of the earlier data collects, it was found that during rotation of the capillary the clumps moved along the capillary and out of the beam. Subsequent samples were prepared by packing a few mm of small clumps in a 0.5 mm quartz capillary then inserting a 0.3 mm capillary to the edge of the specimen, to stop any movement. The data collections were conducted on the powder diffraction beamline at the Australian Synchrotron (Wallwork *et al*., 2007). High energy 21 keV X-rays were used to reduce fluorescence due to As. The wavelength was 0.59028(6) Å, calibrated to NIST standard LaB_6 660b. The capillary was positioned in the diffractometer rotation centre and spun at ca. 1 Hz. The X-ray beam was

aligned to coincide with the diffractometer centre and slits were used to restrict the beam width to 2 mm. The data were collected using a Mythen position sensitive detector (Schmitt *et al*., 2003) covering 80° in 2θ with a step size of 0.00375° in 2θ. Heating was supplied by an Oxford Cryostream system. The first data collection was at close to ambient (25°C). The temperature was then increased in steps of 25°C to 100°C and at each temperature pairs of data sets were collected at two detector positions 0.5° apart in order to cover the gaps between the detector modules. Acquisition time at each position was 300 seconds. The data pairs were merged into single files using in-house data processing software, PDViPcR, available at the beamline. After the 100°C collect the sample was cooled to ambient and a dataset obtained. A dataset was also collected on an empty capillary so that correction for the capillary contribution could be applied in the calculation of pair distribution functions (PDF) from the datasets.

Le Bail fitting of the PXRD data to obtain refined unit cell parameters was made using JANA2006 (Petříček *et al*., 2014). Manual backgrounds were used with interpolation between 40 points and a pseudo-Voigt peak shape function. It was necessary to include a parameter for selective peak broadening for reflections with $h = 2n+1$.

Pair distribution functions (PDFs) were generated from the synchrotron datasets, with Q_{max} = 16.9 $Å^{-1}$. The raw diffraction data were corrected for capillary contribution, reduced to structure functions and then Fourier transformed to the PDFs, G(r) (Egami and Billinge, 2003). PDF calculations were conducted using PDFgui (Farrow *et al*., 2007).

Gandolfi PXRD patterns were obtained on small clumps of crystals of the Neubulach type specimen studied by Walenta (1983). The Gandolfi patterns were obtained on a Rigaku XtaLAB Synergy diffractometer at the School of Chemistry, University of Melbourne. The instrument employs a HiPix CCD Plate detector and CuKα radiation.

Transmission electron microscopy

Crystal aggregates were sonicated in ethanol and the suspension was dispersed onto a holey carbon grid for transmission electron microscopy (TEM). The TEM studies were conducted using a JEOL 4000EX microscope with a LaB_6 source and a spherical aberration coefficient of 1.06 mm. The microscope was operated at 400 kV, using parallel illumination geometry to minimise beam damage. TEM images were recorded on a Gatan slow scan CCD camera.

The new technique of low-dose electron diffraction tomography (Kodjikian and Klein, 2019) was applied to crystals from a specimen that had been heated to 100°C and had a PXRD pattern corresponding to bulachite (Walenta, 1983). Crystal aggregates were lightly crushed in an agate mortar in absolute ethanol and a droplet of the suspension was deposited on carbon-coated copper grid. The ED data collection was made using a Philips CM300ST TEM, equipped with a TVIPS F416 CMOS camera, a Nanomegas Spinningstar device and a Bruker Silicon Drift Detector for EDS. The diffraction intensities were measured on one selected particle (atomic composition from EDS: Al:64.6% and As: 35.3%, Oxygen was detected but not quantified). The tilt step between two frames of the tomography was chosen as 1°, the precession angle was 1.05°. A data set of 105 frames with an exposure time of 0.5 s per frame was recorded from a single crystal of approximate size of 1 µm * 0.5 µm. During the automated data acquisition the beam was blanked from the sample between the exposures in order to irradiate the crystal only during the exposure time of the diffraction patterns. The dose rate was 0.056 electrons.s^{-1}.$Å^{-2}$ and the total dose was 3 electrons.$Å^{-2}$. Data analysis of the recorded patterns was performed with the software PETS2.0 (Palatinus *et al*., 2019) and Jana2006 (Petříček *et al*., 2014).

Crystal structure determinations

The crystal structure of the sample heated to 100°C (= bulachite) was independently solved from the low-dose electron diffraction tomography data and from the synchrotron PXRD data. The individual ED patterns of the tomography series were treated for data reduction in PETS

2.0. Sections of the reciprocal lattice showed reflection conditions leading to the extinction symbol *Pn-a* consistent with space groups *Pnma* and $Pn2_1a$.

Superflip in JANA2006 (Petříček *et al*., 2014) was used to obtain a model in space group $Pn2_1a$ from the PXRD data whereas the ED data were used in Superflip and in SIR2014 (Burla *et al*., 2015) where both space groups were tested and the best fit was found for a *Pnma* model. Both the ED and PXRD-derived models had the same topology of edge-shared Al-centred octahedra connected to AsO_4 tetrahedra by corner-sharing. Based on the ED model, a centre of symmetry was located for the $Pn2_1a$ model and the atomic coordinates were transformed to the centrosymmetric space group setting for refinement against the synchrotron PXRD data.

The crystal structure of the higher-hydrate mineral was established by recognising that it had the same polyhedral layers as in bulachite, but with an increased layer separation due to the presence of interlayer water molecules. The *x* coordinates for the bulachite model were scaled by the ratio of the two *a* axes to establish the polyhedral layers in the a = 19.9 Å cell. The PXRD pattern for this model was calculated and found to have only a fair agreement with the experimental pattern. We examined the possibility that the transformation of the a = 19.9 Å phase to the a = 15.4 Å phase involved not only a contraction of the interlayer spacing but also a sliding of the layers relative to one another, as we found in heating studies on other hydrated aluminium arsenate minerals (Grey *et al*., 2016*b*). In space group *Pnma*, the layers can be displaced relative to one another along [001], with no distortion of the polyhedra, by changing the *z* coordinate for all atoms by the same amount. We ran a series of tests where the *z* coordinate for all atoms was changed in increments of 0.01. It was found that changing *z* in a positive sense improved the fit to the experimental PXRD pattern, and the profile *R* factors decreased with increasing Δz up to 0.09 then increased with further change in *z*. The value of Δz was then fixed at 0.09, and difference-Fourier maps were used to locate the interlayer water molecules.

Structure refinements

The *Pnma* structural model for bulachite was refined both with the synchrotron PXRD data and by dynamical refinement of the ED data. The latter will be reported separately. Here we describe the PXRD refinement, using the synchrotron data to a resolution of 1.0 Å (the peaks become very weak and broad at higher resolutions). The Rietveld data collection and refinement conditions are given in Table 1.

The profile parameters were established using a Le Bail structureless fit to the PXRD pattern. Manual backgrounds were automatically located at 40 positions in JANA2006. The unit-cell parameters, a zero-shift, the Lorentzian parameters *LX* and *LY*, and a parameter to deal with anisotropic peak broadening for reflections *hkl* with $h = 2n+1$ were refined, giving Le Bail fit indices of Rp = 2.60, Rwp = 3.73 and Goodness of fit, *GoF* = 3.13.

The atomic coordinates were refined using soft distance restraints for the As−O and Al−O distances of 1.670(1) Å and 1.900(5) Å, respectively. The restrained distances used are the mean of As−O and Al−O distances obtained from single-crystal refinements of other aluminium arsenate minerals (Grey *et al*., 2013, 2015, 2016*a*). Angle restraints were also used, for the AsO_4 tetrahedra, O−As−O = 109.47(2)°. Group isotropic displacement parameters, *B*, for the metal atoms, polyhedral anions and interlayer water molecule oxygen atoms were refined. Rietveld refinement in JANA2006 converged at fit indices of Rp = 3.73, Rwp = 5.09 and *GoF* = 4.29. The refined structural parameters are reported in Table 2. The atom labels are the same as used for other hydrated Al arsenate minerals (Grey *et al*., 2015, 2016a) where OH = hydroxyl, Ow = coordinated H_2O and *W* = H-bonded H_2O. Polyhedral bond distances, cation-cation distances and likely H-bonded pairs are given in Table 3.

For the higher-hydrate mineral the structural parameters were not refined, apart from establishing the magnitude of layer sliding along [001] as discussed above. The synchrotron PXRD pattern for this mineral (Figure 1) is of lower quality than that for bulachite. In

particular, all reflections with non-zero *h* are broadened and the reflections with *h* odd are broader than those with *h* even. This was dealt with by combining anisotropic Lorentzian particle size broadening (parameter *LXe*) with anisotropic peak broadening for reflections with $h = 2n+1$. As for bulachite, the PXRD data was truncated at 1 Å resolution, 40 manual backgrounds were located and profile parameters were established with a Le bail fit, giving fit indices of Rp = 2.88, Rwp = 4.06 and *GoF* = 3.40. The interlayer water molecules were located in difference-Fourier maps. The agreement factors for the Rietveld fitting of the PXRD data are Rp = 5.57, Rwp = 7.43 and *GoF* = 6.23. Because the polyhedral layers are built from the refined bulachite structure, the polyhedral bond distances are the same as reported in Table 2 for bulachite. The higher hydrate is a potential new mineral and further crystallochemical details await the preparation of a new mineral proposal to the International Mineralogical Association Commission on New Minerals, Nomenclature and Classification (IMA−CNMNC).

Results

The low-angle region of the PXRD pattern for the Cap Garonne specimen is shown in Figure 3. The indexed sharp peaks in the pattern are also present in the bulachite pattern reported by Walenta (1983) but the other peaks, which are much broader, have no counterpart in the bulachite pattern. The sharp reflections all correspond to a single reciprocal lattice section, (0*kl*). This was the most commonly encountered pattern in ED studies of the sample. The ED (0*kl*) pattern is shown in Figure 4a. It is obtained when the platy laths lie flat on the TEM grid. Indexing of the ED pattern gives cell parameters b = 17.7 Å and c = 7.8 Å. Systematic absences in the pattern for (0*kl*) reflections with $k+l = 2n+1$ indicate an *n*-glide plane. The associated image of the diffracting crystal is shown in Figure 4b. It confirms that the direction of the 7.8 Å axis is parallel to the long dimension of the lath. Aided by the ED results the PXRD could

be fully indexed and a Le Bail refinement gave the orthorhombic unit-cell parameters a = 19.849(2), b = 17.6903(4) and c = 7.7788(3) Å, with possible space groups *Pnma* or $Pn2_1a$.

PXRD patterns corresponding to heating of the Cap Garonne specimen are presented in Figure 5. At 50°C there is the appearance of a peak at d = 7.8 Å (arrowed), which is the strongest peak in the pattern of bulachite (Walenta, 1983). Note that this peak is present in the room temperature pattern but it is very weak and broad. At 75°C there is a dramatic change in the pattern with a strong increase in the 7.8 Å peak and a marked diminution in the 10 Å peak and other peaks present in the room temperature pattern. At 100°C the transformation is complete and all peaks present match those reported by Walenta (1983) for bulachite.

ED patterns obtained on the sample heated to 100°C were indexed with unit-cell parameters a = 15.4, b = 17.7 and c = 7.8 Å. Using these as starting parameters in a Le Bail fit to the 100°C PXRD pattern gave the refined unit cell parameters a = 15.3994(3), b = 17.6598(3) and c = 7.8083(1) Å. The systematic extinctions in the ED patterns correspond to space groups *Pnma* or $Pn2_1a$, the same as for the a = 19.9 Å mineral. As mentioned in the previous section the fit indices were Rp = 2.60, Rwp = 3.73 and *GoF* = 3.13. For comparison we re-ran the Le Bail fitting to the 100°C dataset starting with the unit cell parameters reported by Walenta (1983). There was a marked deterioration to the fit, with fit indices Rp = 6.17, Rwp = 10.49 and *GoF* = 9.76. With the higher resolution of the synchrotron data (Walenta used a Debye-Scherrer camera with Fe$K\alpha$. radiation), serious misfits are evident using the Walenta cell, due to the incorrect c parameter.

The possibility existed that the bulachite specimen from Cap Garonne was crystallochemically different from the bulachite from Neubulach. To check this we obtained a portion of the specimen characterised by Walenta (1983). We were able to confirm, by obtaining Gandolfi PXRD patterns on different crystal aggregates, that both the a = 19.9 Å and a = 15.4 Å phases are present in the Neubulach sample, as shown in Figure 6. For the 19.9 Å phase, the reflections

involving *h* are very broad, including the strong characteristic (200) reflection at *d* ~ 10 Å, so small amounts of this phase are difficult to detect. Frau and da Pelo (2001) noted that their PXRD pattern had an anomalously high background suggestive of the presence of amorphous phase and broad peaks. Our PXRD heating experiments (Figure 5) show that the 19.9 Å phase begins to transform to bulachite within a few minutes at 50°C, so it is likely that at suitable humidity conditions, the transformation could occur at ambient temperatures over long periods. The dehydration of the 19.9 Å phase will start at the surface of the mineral crusts and move inwards under diffusion control, so it is not unexpected to find a mix of the two phases in the crusts. It is possible that the specimen that Walenta used to obtain a PXRD pattern came from the upper region of the surface aggregates where dehydration of the 19.9 Å phase had occurred.

As described in the Experimental section, the crystal structure of bulachite was determined in space group *Pnma* using low-dose electron tomography data and refined using Rietveld treatment of synchrotron PXRD data. The data collection and refinement details are given in Table 1 and the Rietveld fit to the PXRD data is shown in Figure 7.

Projections of the crystal structures along the 7.8 Å axis are shown in Figures 8 and 9 for bulachite and the higher hydrate, respectively, while Figure 10 shows a view of the structures normal to the (100) layers. This Figure shows that the polyhedral layers are built from edge-shared Al-centred octahedra that form spiral chains along [001], the same as occurs in liskeardite (Grey *et al*., 2013). The spirals are joined together along [010] by edge-sharing of octahedra in the mirror plane at $y = ¼$. The spirals are decorated with AsO_4 tetrahedra that corner-connect to the AlO_6 octahedra in the same manner as in liskeardite.

The close relationship of the two structures to that of liskeardite is illustrated by comparing the PDFs for the three minerals in Figure 11. The first three strong peaks in the PDFs, at 1.8. 2.7 and 3.2 Å correspond to As−O + Al−O, O−O and As−Al + Al−Al distances, respectively.

The O−O at 2.7 Å is strong despite the low scattering of oxygen, because fortuitously the O−O distances in both the AsO_4 tetrahedra and the AlO_6 octahedra are almost the same.

The composition of the layers is readily established from the refinement using bond valence sums (BVS) to distinguish the different anions. BVS values were calculated using the parameters of Gagné and Hawthorne (2015). The values, in valence units, are given in Table 2. Taking into account the site multiplicities, they show clearly that the layers contain 12 oxygens, 9 hydroxyls and 4 coordinated H_2O. The O2 and O6 sites, which contain unshared tetrahedral oxygen atoms, have low BVS values of 1.32, while the sites O4 and O7 are also slightly low. However, as shown by the H-bond couples in Table 3, oxygen atoms at these sites are acceptor atoms for several H-bonds from OH, Ow and *W* donor atoms. Taking into account the numbers of O, OH and Ow gives the layer formula $Al_6(AsO_4)_3(OH)_9(H_2O)_4$, with Z = 4. The same layer formula applies to the higher hydrate mineral. Adding in the H-bonded H_2O (=*W*) gives the overall formula for bulachite of $[Al_6(AsO_4)_3(OH)_9(H_2O)_4]\cdot 2H_2O$, while the formula for the higher hydrate is $[Al_6(AsO_4)_3(OH)_9(H_2O)_4]\cdot 8H_2O$.

A search of the literature failed to find any related PXRD pattern or unit cell that matched those for the higher hydrate. The Cap Garonne specimen appears to be a new mineral which eventually will require a proposal to be prepared to the IMA−CNMNC for validation.

Acknowledgments

We thank Robert Gable for help in obtaining the Gandolfi patterns, Matthew Glenn for the SEM image, Anita d'Angelo for help with the synchrotron PXRD data collects. Thanks also to Vaclav Petříček for help in the use of JANA2006. Part of this research was undertaken at the powder diffraction beamline at the Australian Synchrotron, Victoria, Australia. We appreciate the thorough checking of our manuscript by Luca Bindi and two other reviewers.

References

Burla, M.C., Caliandro, R., Carrozzini, B., Cascarano, G.L., Cuocci, C., Giacovazzo, C., Mallamo, M., Mazzone, A. and Polidori, G. (2015) Crystal structure determination and refinement via SIR2014. *Journal of Applied Crystallography*, **48**, 306─309.

Egami, T. and Billinge, S.J.L. (2003) Underneath the Bragg Peaks. London: Pergamon.

Farrow, C.L., Juhás, P., Liu, J.W., Bryndin, D., Božin, E.S., Bloch, J., Proffen, Th. and Billinge, S.J.L. (2007) PDFfit2 and PDFgui: computer programs for studying nanostructure in crystals, *Journal of Physics. Condensed Matter*, **19**, 335219.

Favreau, G. and Galea-Clolus, V (2014) Cap Garonne. Association Française de Microminéralogie, Carry-le-Rouet, France.

Frau, F. and Da Pelo, S. (2001) Bulachite, a rare aluminium arsenate from Sardinia, Italy: the second world occurrence. *Neues Jahrbuch für Mineralogie, Monatshafte*, **2001**, 18─26.

Gagné, O.C. and Hawthorne, F.C. (2015) Comprehensive derivation of bond-valence parameters for ion pairs involving oxygen. *Acta Crystallographica*, **B71**, 562–578.

Grey, I.E., Mumme, W.G., MacRae, C.M., Caradoc-Davies. T., Price, J.R., Rumsey, M.S. and Mills, S.J. (2013) Chiral edge-shared octahedral chains in liskeardite, $[(Al,Fe)_{32}(AsO_4)_{18}(OH)_{42}(H_2O)_{22}]\cdot 52H_2O$, an open framework mineral with a pharmacoalumite-related structure. *Mineralogical Magazine*, **77**, 3125−3135.

Grey, I.E., Mumme, W.G., Price, J.R., Mills, S.J., MacRae, C.M. and Favreau, G. (2014) Ba−Cu ordering in bariopharmacoalumite-*Q2a2b2c* from Cap Garonne, France. *Mineralogical Magazine*, **78**, 851−860.

Grey, I.E., Kampf, A.R., Price, J.R. and MacRae, C.M. (2015) Bettertonite, $[Al_6(AsO_4)_3(OH)_9(H_2O)_5]\cdot 11H_2O$, a new mineral from the Penberthy Croft mine, St. Hilary, Cornwall, UK, with a structure based on polyoxometalate clusters. *Mineralogical Magazine*, **79**, 1849−1858.

329 Grey, I.E., Betterton, J., Kampf, A.R., MacRae, C.M., Shanks, F.L. and Price, J.R. (2016a)
330 Penberthycroftite, $[Al_6(AsO_4)_3(OH)_9(H_2O)_5]\cdot 8H_2O$, a second new hydrated aluminium
331 arsenate minerals from the Penberthy Croft mine, St. Hilary, Cornwall, UK. *Mineralogical*
332 *Magazine*, **80**, 1149−1160.
333 Grey, I.E., Brand, H.E.A. and Betterton, J. (2016b) Dehydration phase transitions in new
334 aluminium arsenate minerals from the Penberthy Croft mine, Cornwall, UK. *Mineralogical*
335 *Magazine*, **80**, 1205─1217.
336 Kodjikian, S. and Klein, H. (2019) Low-dose electron diffraction tomography (LD-EDT)*.
337 *Ultramicroscopy*, **200**, 12─19.
338 Palatinus, L., Brazda, P., Jelinek, M., Hrda, J., Steciuk, G. and Klementova, M. (2019)
339 Specifics of the data processing of precession electron diffraction tomography data and their
340 implementation in the program PETS2.0. *Acta Crystallographica* **B**, **75,** 512-522.
341 Petříček, V., Dušek, M., and Palatinus, L. (2014) Crystallographic Computing System
342 JANA2006: General features. *Zeitschrift für Kristalloraphie.*, **229**, 345−352.
343 Schmitt, B., Bronnimann, C., Eikenberry, E.F., Gozzo, F., Hormann, C., Horisberger, R. and
344 Patterson, B. (2003) Mythen detector system. *Nuclear Instruments and Methods in Physics*
345 *Research*, **A501**, 267−272.
346 Walenta, K. (1983) Bulachit, ein neues Aluminiumarsenatmineral von Neubulach im
347 nördlichen Schwarzwald. *Aufschluss*, **34**, 445─451.
348 Wallwork, K.S., Kennedy, B.J. and Wang, D. (2007) The high resolution powder diffraction
349 beamline for the Australian Synchrotron, *AIP Conference Proceedings*, **879**, 879–882.
350

Table 1. Synchrotron PXRD data collection and Rietveld refinement details for bulachite.

Formula	$[Al_6(AsO_4)_3(OH)_9(H_2O)_4]\cdot 2H_2O$
Unit-cell parameters (Å)	a = 15.3994(3) b = 17.6598(3) c = 7.8083(1)
Volume (Å^3), Z	2123.46(7), 4
Space group	*Pnma*
X-ray radiation source, wavelength (Å)	Australian Synchrotron, 0.59028(6)
2θ range, step size (°)	1.50 to 104.82, 0.00375
Resolution for structure analysis (Å), number of contributing reflections	1.0, 1158
Number of profile parameters	8
Number of structural parameters/restraints	63/38
Profile function	Pseudo-Voigt
Background	Interpolation between 40 selected points
Rp, Rwp, GoF, R_F	3.73, 5.09, 4.29, 10.7

Table 2. Refined atomic coordinates, isotropic displacement parameters and calculated bond valence sums (BVS) for bulachite.

Atom	*x*	*y*	*z*	*B* (Å^2)	BVS
As1	0.82245(18)	0.00921(19)	0.3827(4)	0.0368(6)	5.22
As2	0.9057(3)	0.25	0.5824(6)	0.0368(6)	5.24
Al1	0.6329(6)	0.0696(5)	0.2444(17)	0.0368(6)	3.11
Al2	0.8397(6)	0.0964(5)	0.7535(16)	0.0368(6)	2.96
Al3	0.7207(6)	0.1692(6)	0.4971(16)	0.0368(6)	2.70
O1	0.7276(5)	-0.0061(6)	0.2856(14)	0.0186(15)	2.19
O2	0.9002(6)	0.0190(6)	0.2359(12)	0.0186(15)	1.32
O3	0.8160(7)	0.0885(5)	0.5006(13)	0.0186(15)	2.00
O4	0.8459(7)	-0.0642(5)	0.5099(13)	0.0186(15)	1.86
O5	0.8043(5)	0.25	0.5078(18)	0.0186(15)	2.28
O6	0.9752(8)	0.25	0.4186(14)	0.0186(15)	1.32
O7	0.9217(6)	0.17267(14)	0.7019(7)	0.0186(15)	1.82
OH1	0.7085(9)	0.1522(7)	0.250(2)	0.0186(15)	0.98
OH2	0.6300(10)	0.0952(9)	0.4819(19)	0.0186(15)	0.98
OH3	0.9259(8)	0.0208(7)	0.772(3)	0.0186(15)	1.10
OH4	0.7386(8)	0.1541(7)	0.740(2)	0.0186(15)	1.01
OH5	0.6390(13)	0.25	0.511(3)	0.0186(15)	1.00
Ow1	0.5229(9)	0.1135(7)	0.226(3)	0.0186(15)	0.55
Ow2	0.8415(13)	0.1119(9)	0.9944(19)	0.0186(15)	0.51
*W*1	0.93	0.25	0.018	0.074(11)	
*W*2	0.3652	0.75	0.0187	0.074(11)	

368 Table 3. Polyhedral bond distances, cation-cation distances and likely H-bonded pairs in
369 bulachite.
370

As1−O1	1.667(8)	Al2−O1	1.918(13)
As1−O2	1.667(9)	Al2−O3	2.014(16)
As1−O3	1.679(9)	Al2−O7	1.890(11)
As1−O4	1.672(10)	Al2−OH3	1.889(16)
Mean	1.671	Al2−OH4	1.864(16)
As2−O5	1.666(10)	Al2−Ow2	1.900(19)
As2−O6	1.668(12)	Mean	1.912
As2−O7	1.673(5)	Al3−O3	2.046(14)
Mean	1.670	Al3−O5	1.924(11)
Al1−O1	2.005(13)	Al3−OH1	1.96(2)
Al1−O4	1.862(17)	Al3−OH2	1.917(18)
Al1−OH1	1.868(15)	Al3−OH4	1.94(2)
Al1−OH2	1.91(2)	Al3−OH5	1.905(17)
Al1−OH3	1.847(15)	Mean	1.949
Al1−Ow1	1.869(16)		
Mean	1.894	As1−Al1	3.290(10)
Potential H-bonded pairs		As1−Al1	3.223(13)
Donor…Acceptor		As1−Al2	3.291(12)
Ow1…O2	2.55	As1−Al2	3.276(10)
Ow1…O4	2.77	As1−Al3	3.352(10)
Ow1---O6	2.77	As2−Al2	3.190(10)
Ow2…O2	2.65	As2−Al2	3.190(10)
Ow2…O4	2.99	As2−Al3	3.255(10)
Ow2…O7	2.82	As2−Al3	3.255(10)
*W*1…O7	2.82	Al1−Al2	2.962(12)
*W*2…O6	2.58	Al1−Al3	2.970(16)
OH2…O2	2.84	Al2−Al3	3.004(15)
OH3…O2	2.79	Al3−Al3	2.854(14)
OH4…O4	2.92		
OH4…O7	2.86		
OH5…O2	2.55		
OH5…O4	2.77		
OH5…O6	2.77		

371

Figure 1. Patchy regions of bulchite (white) on yellow pharmacoalumite from Cap Garonne. FOV 15 mm. Museums Victoria specimen M55455.

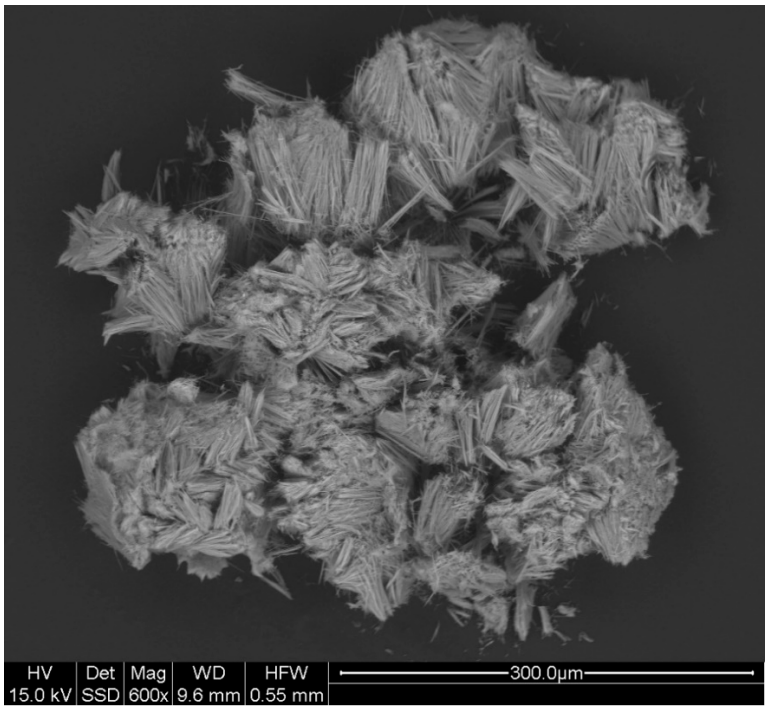

Figure 2. SEM back-scattered electron image of clumps of fibrous bulachite crystals from Cap Garonne. Museums Victoria specimen M55455.

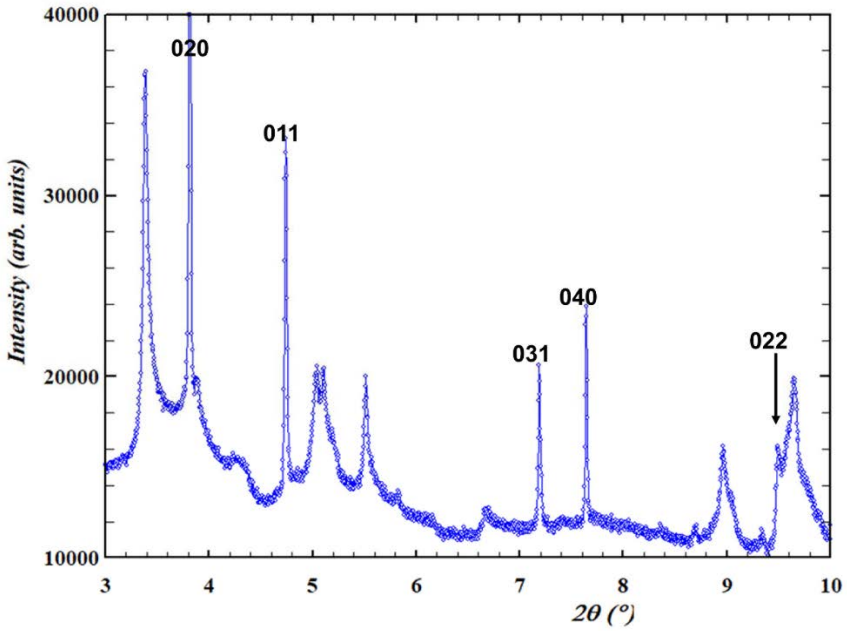

Figure 3. Low-angle region of the synchrotron PXRD pattern for the Cap Garonne specimen. The sharp reflections all index as (0*kl*) based on cell parameters *b* = 17.7 and *c* = 7.8 Å. The first reflection is (200) where *a* = 19.9 Å.

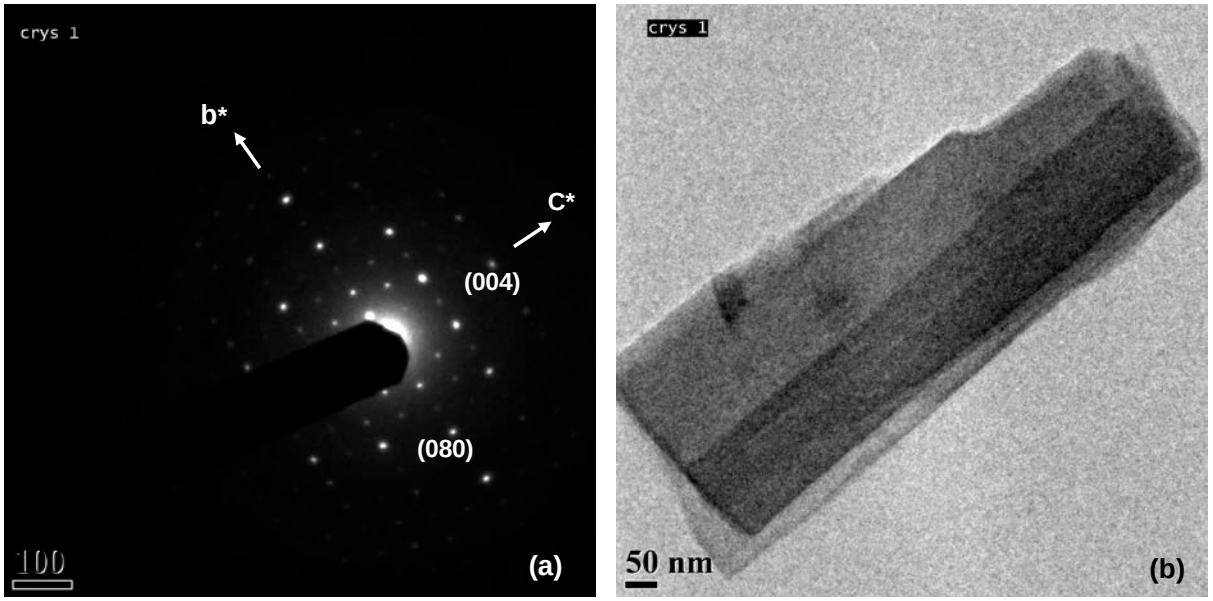

Figure 4. Electron diffraction (0*kl*) reciprocal lattice section for the Cap Garonne specimen. (b) Image of flat lath crystal used to obtain the ED pattern. Museums Victoria specimen M55455.

Figure 5. Low-angle region of synchrotron PXRD patterns for the Cap Garonne specimen heated at temperatures 25, 50, 75 and 100°C. Indexing of the 100°C pattern shown.

Figure 6. Gandolfi PXRD patterns for two separate tufts of the Neubulach type specimen of bulachite (Cu*K*α radiation).

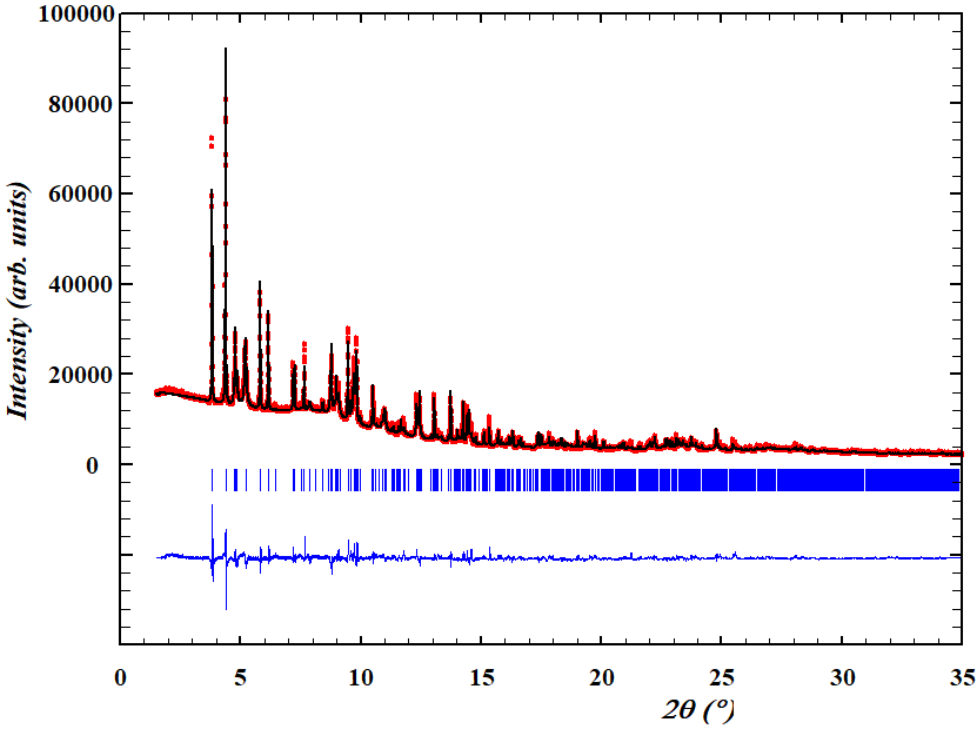

Figure 7. Rietveld observed (red points) and calculated (black line) PXRD patterns for bulachite from Cap Garonne. Short bars show the positions of the Bragg reflections. The difference plot is in blue.

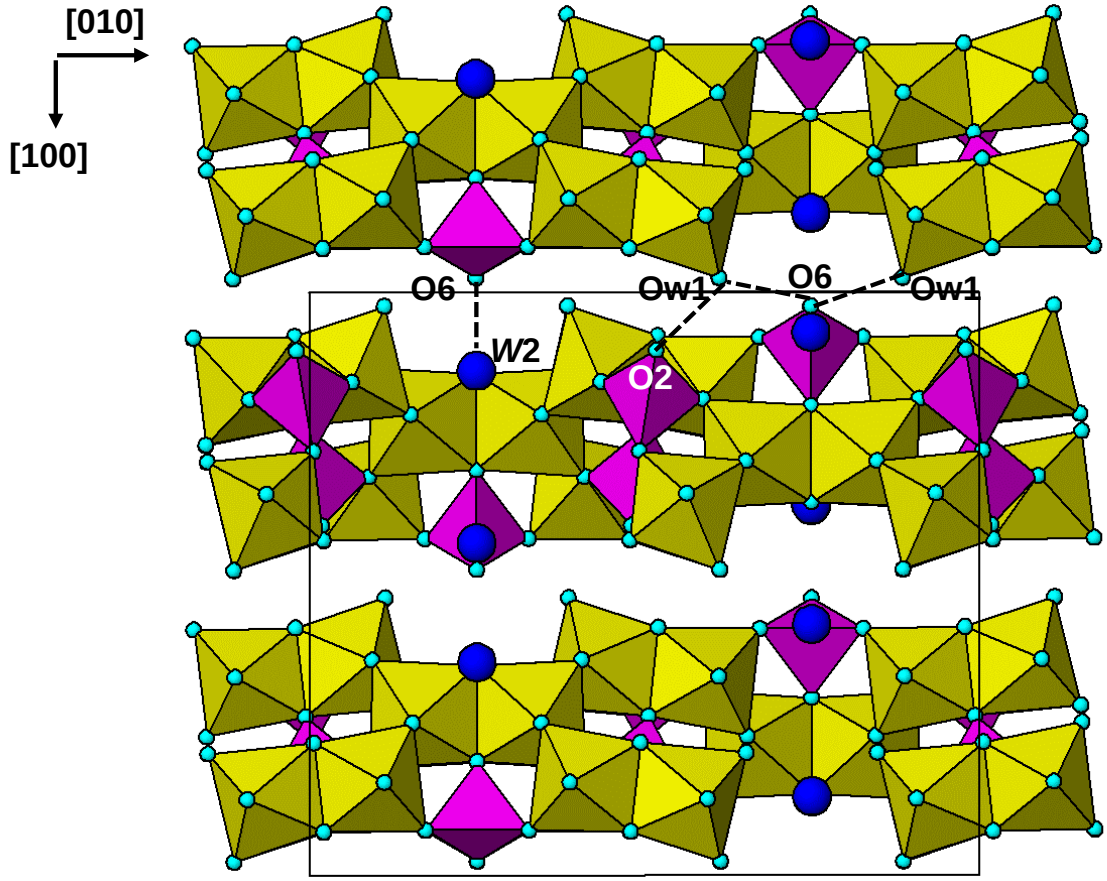

Figure 8. [001] projection of the layer structure for bulachite. Dotted lines show likely interlayer H-bonds. Dark blue spheres are water molecules, Al-centred octahedra are yellow and AsO_4 tetrahedra are mauve.

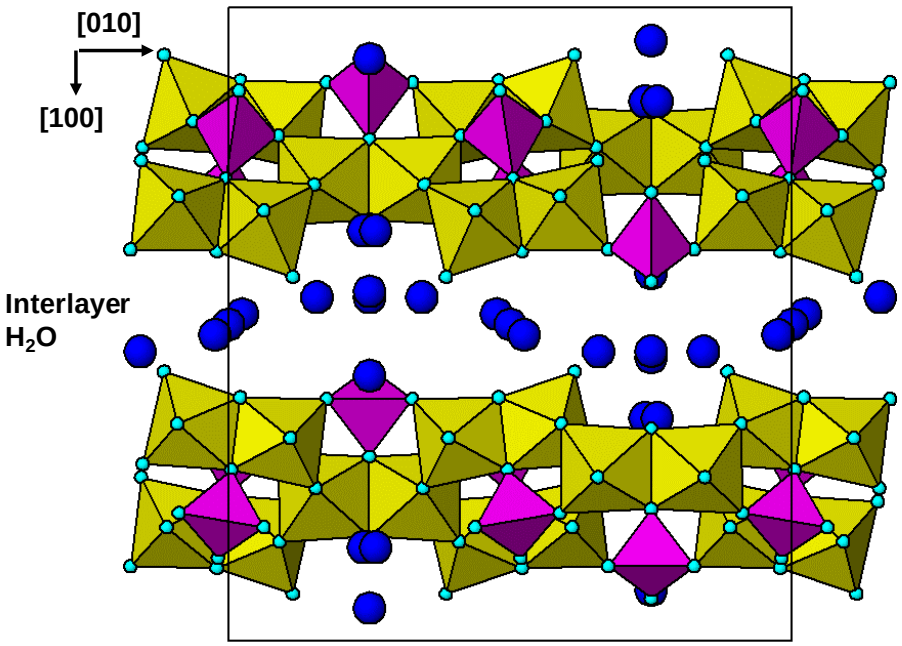

Figure 9. [001] projection of the layer structure for the higher hydrate mineral. Blue spheres are interlayer water molecules, Al-centred octahedra are yellow and AsO_4 tetrahedra are mauve.

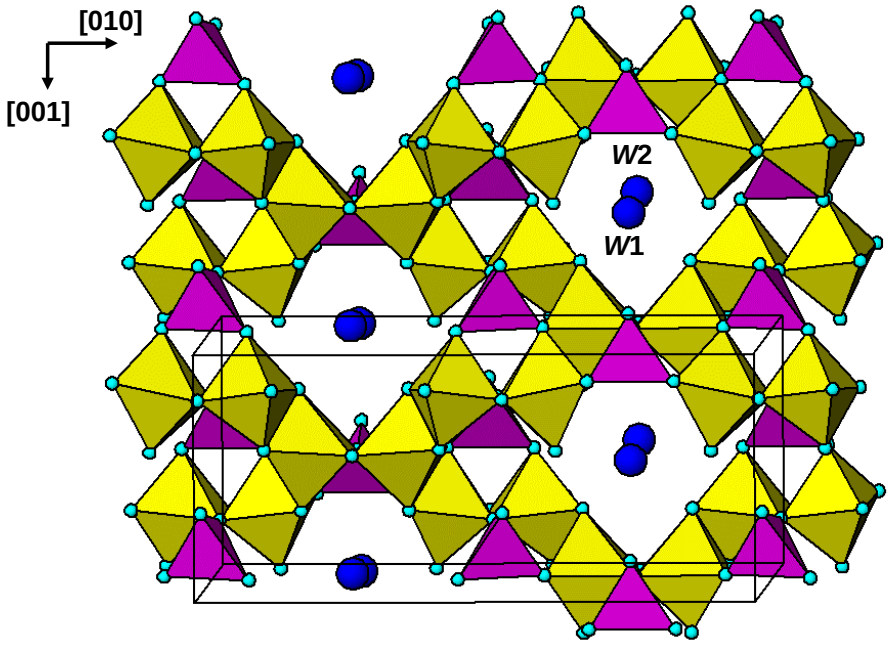

Figure 10. Projection approximately along [100] of the structure of bulachite, showing spirals along [001] of edge-shared Al-centred octahedra (yellow) and corner-connected AsO_4 tetrahedra (mauve).

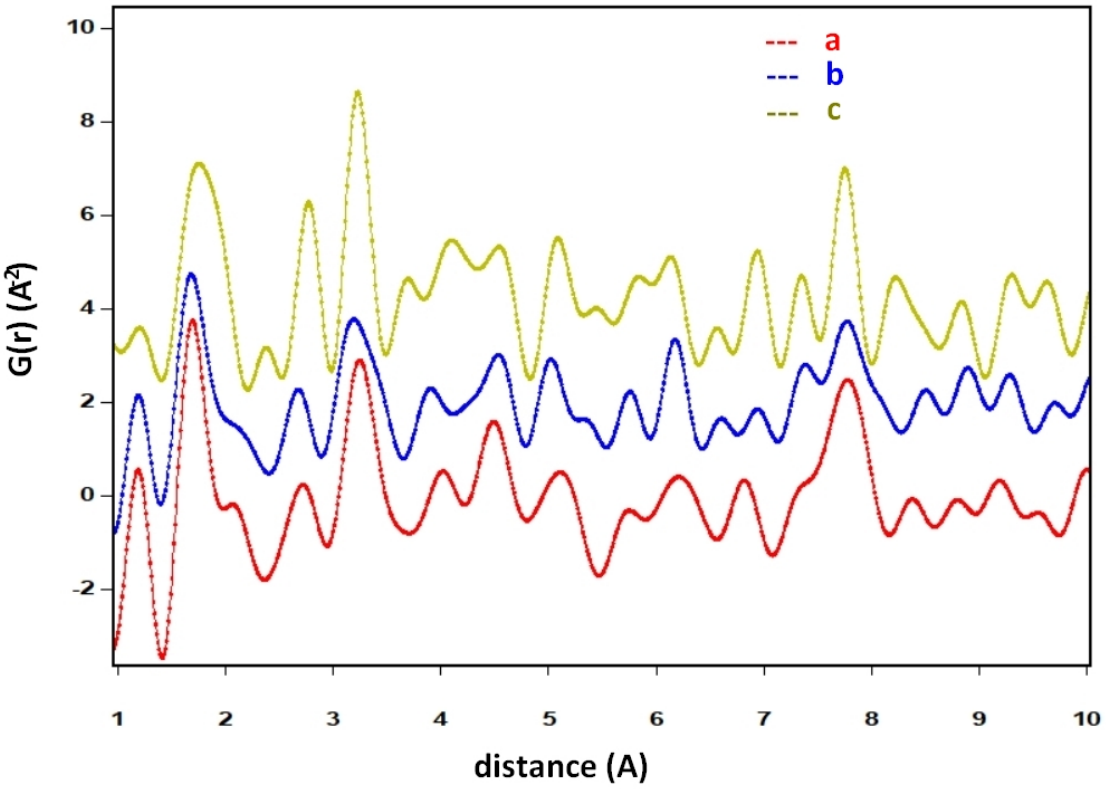

Figure 11. Experimental PDFs for (a) the higher hydrate mineral and (b) bulachite formed at 100°C, compared with the calculated PDF for liskeardite (c).